ACS OMEGA

http://pubs.acs.org/journal/acsodf

Article

Mechanism of Elastic Properties of Biodegradable Poly[(*R*)-3-Hydroxybutyrate-*co*-4-hydroxybutyrate] Films Revealed by Synchrotron Radiation

Yuki Kawamura, Hongyi Gan, Taizo Kabe, Akira Maehara, Satoshi Kimura, Takaaki Hikima, Masaki Takata, and Tadahisa Iwata*

Cite This: *ACS Omega* 2021, 6, 7387−7393

Read Online

ACCESS | Metrics & More | Article Recommendations

ABSTRACT: Reversible elastic films of biobased and biodegradable poly[(*R*)-3-hydroxybutyrate-*co*-4-hydroxybutyrate] [P(3HB-*co*-4HB)] were prepared by uniaxial drawing procedures. Mechanical properties and highly ordered film structures were investigated by tensile testing and both static-state and *in situ* wide-angle X-ray diffraction and small-angle X-ray scattering with synchrotron radiation during stretching and relaxing. Despite the crystalline nature of the polymers, the elongation at break of these films was greater than 1500%. Reversible elasticity was achieved after the first 10 times of uniaxial stretching. X-ray measurement results indicated that on stretching, β-form molecular chains with a planar zigzag conformation were introduced from molecular chains with random coils in the amorphous regions between α-form lamellar crystals. Notably, the orientation of the α-form lamellar crystals increased after relaxation of the molecular chains with a planar zigzag conformation (β-form) between the lamellar crystals (α-form). Reversible elastic properties were regenerated by a planar zigzag conformation between the lamellar crystals, the extension of molecular chains in lamellar crystals by the rotation of molecular conformation, and changes in the degree of orientation of the lamellar crystals.

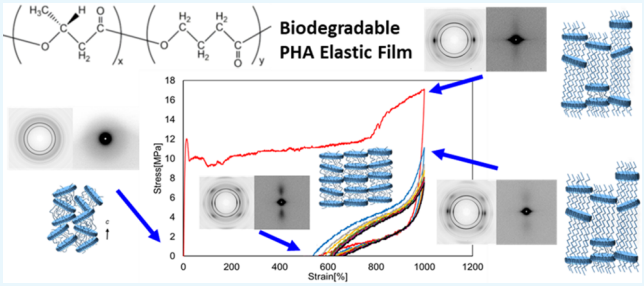

INTRODUCTION

Polyhydroxyalkanoate (PHA) is a group of biopolymers, which are produced by a wide variety of microorganisms as an energy storage material.[1] P(3HB) is the most extensively studied PHA and is an environmentally biodegradable and biocompatible thermoplastic with a high melting temperature of 180 °C and tensile strength (40 MPa) as high as that of poly(propylene).[2−5] Recently, PHA has attracted much attention as a biodegradable material, which might address the problems associated with marine microplastic pollution. However, from the viewpoint of industrial applications, the elongation at break of P(3HB) homopolymer films deteriorates to 5% owing to secondary crystallization attributable to a low glass transition temperature of 4 °C.[6,7] Accordingly, P(3HB) is copolymerized with other monomer components for industrial applications.

To date, poly[(*R*)-3-hydroxybutyrate-*co*-(*R*)-3-hydroxyvalerate] [P(3HB-*co*-3HV)],[8−11] poly[(*R*)-3-hydroxybutyrate-*co*-(*R*)-3-hydroxyhexanoate] [P(3HB-*co*-3HHx)],[12−14] and poly[(*R*)-3-hydroxybutyrate-*co*-4-hydroxybutyrate] [P(3HB-*co*-4HB)][8,15−19] have been developed (Figure 1). However, unfortunately, in the case of P(3HB-*co*-3HV), 3HV units are included in the P(3HB) crystal, and co-crystallization occurs. As a result, secondary crystallization, similar to that of the case of the P(3HB) homopolymer, also progresses. Conversely, in the case of P(3HB-*co*-3HHx) and P(3HB-*co*-4HB), the co-monomer units 3HHx and 4HB do not enter into the P(3HB) crystals. These crystallization phenomena are well understood through the exclusion model in crystallization. The physical properties of the materials change from brittle to ductile. For example, the elongation at break of P(3HB-*co*-12 mol %-3HHx) and P(3HB-*co*-8 mol %-4HB) films has been reported to be *ca.* 400% with a tensile strength of 20 MPa when secondary crystallization is suppressed.

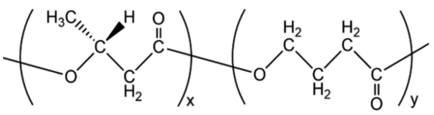

Figure 1. Chemical structure of P(3HB-*co*-4HB).

Received: November 20, 2020
Accepted: February 18, 2021
Published: March 12, 2021

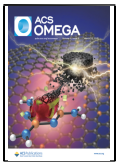

Table 1. 4HB Ratio, M_w, PDI, Thermal Properties, and Mechanical Properties of P(3HB-*co*-4HB)

4HB ratio (%)	M_w ($\times 10^4$)	PDI	T_g (°C)	T_m (°C)	tensile strength (MPa)	elongation at break (%)	Young's modulus (GPa)
16	88	4	−6	140	19.0 ± 1.4	1800 ± 150	0.14 ± 0.01

Iwata et al. developed new drawing methods, such as cold-drawing and two-step cold-drawing, to avoid the secondary crystallization and process high-tensile-strength films of PHA materials, including P(3HB), P(3HB-*co*-3HV), and P(3HB-*co*-3HHx). Highly oriented uniaxially cold-drawn films with a tensile strength of *ca.* 100−150 MPa were successfully prepared. It was confirmed that the mechanical properties of these polymers remained unchanged during storage for 4 months. These increased mechanical properties and stability are mainly attributed to the increase in the orientation of the lamellar crystals and crystallinity.

The X-ray fiber diagrams of P(3HB) films and fibers indicated the existence of two types of molecular conformations. P(3HB) typically crystallizes in an orthorhombic crystal system: α-forms with unit cell parameters of a = 0.576 nm, b = 1.320 nm, and c (fiber axis) = 0.596 nm and the space group of $P2_12_12_1$, where the molecular chains have a 2_1 helix conformation.[20,21] Conversely, when two-step drawing is applied to P(3HB) films and fibers, a new molecular structure is generated based on a planer zigzag conformation (β-form).[22−25] The β-forms were first observed in the drawing of uniaxially stretched P(3HB) homopolymer films by Yokouchi et al.,[20] and this conformation was confirmed in a cold-drawn film of P(3HB-*co*-3HV) films by Orts et al.[11] They calculated the fiber repeat distance and simulated the molecular conformation of the β-forms and revealed that the β-form has a planar zigzag conformation with a fiber repeat distance of 0.920 nm. Furthermore, they proposed that the extended chain conformation (β-form) was generated from noncrystalline domains by cold-stretching. Our group further observed that this planar zigzag conformation was generated from amorphous regions between lamellar crystals of α-forms by two-step drawing in strong films and fibers. Furthermore, the development of a planar zigzag conformation (β-form) and the highly ordered structure of lamellar crystals avoided deterioration by secondary crystallization. More recently, Tashiro et al. analyzed the three-dimensional crystal structure of the β-form of P(3HB).[26]

The purpose of this study is to prepare reversible elastic films of P(3HB-*co*-4HB) and to reveal the mechanism of reversible elastic behavior through the use of both static-state and *in situ* wide-angle X-ray diffraction and small-angle X-ray scattering by synchrotron radiation.

RESULTS AND DISCUSSION

Properties. Table 1 shows the 4HB ratio, weight average molecular weight (M_w), polydispersity index (PDI), thermal properties, and mechanical properties of the used sample. The 4HB ratio of the samples was 16 mol %, and M_w and PDI were 880 000 and 4, respectively. Based on the NMR measurement, it was found that P(3HB-*co*-16 mol %-4HB) is a random copolymer. Figure 2 shows a typical stress−strain curve of the solvent-cast film. The tensile strength and Young's modulus were 20 MPa and 0.14 GPa, respectively. These values are slightly lower than those of the P(3HB) homopolymer film at 32 MPa and 1.11 GPa, respectively.[23] However, the value of the elongation at break of the P(3HB-*co*-4HB) samples was *ca.* 1800%. In previous studies, the elongation at break of P(3HB-*co*-16 mol %-4HB) was reported to be only 440%.[4] The difference of these values seems to be the difference of random sequence of 4HB units in the copolymer chain. The P(3HB) homopolymer is a hard and brittle material. Such high elongation at break is an attractive property.

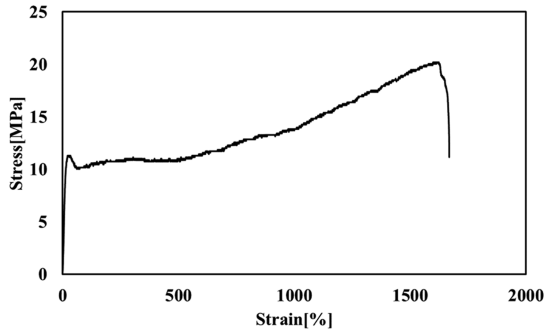

Figure 2. Stress−strain curve of the P(3HB-*co*-16 mol %-4HB) film.

Stress−Strain Cycle Testing. Various drawing ratios from three times to 15 times were applied to solvent-cast films. Reproducible reversible elasticity was found for the P(3HB-*co*-4HB) films after 10 times of drawing of the initial length. Figure 3 shows the sample preparation procedures and reversible elasticity. On the initial drawing ((ii) drawing) of the original samples ((i) Original) to 10 times, the initial length was applied at room temperature. Then, the drawing strength was released to a state of zero stress ((iii) zero stress). When the stress was released, the film shrank in length to be five or six times the initial length. Such reversible elastic behavior was generated in the zero-stress film. The zero-stress film was easily stretched again up to 10 times at room temperature ((iv) drawing again).

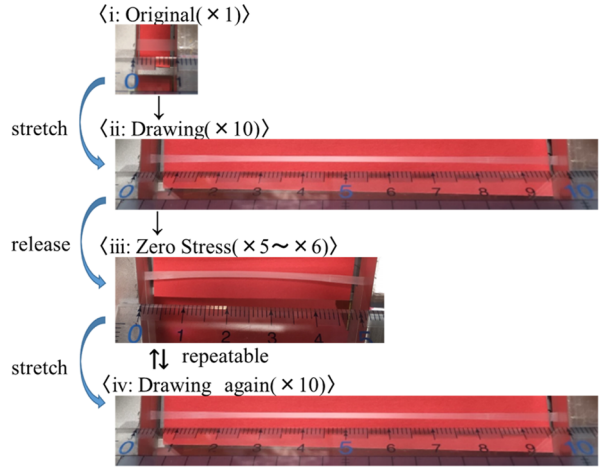

Figure 3. Drawing process of P(3HB-*co*-16 mol %-4HB) films. ⟨(i) Original (×1)⟩ indicates a predrawn state, ⟨(ii) drawing (×10)⟩ indicates a film drawn to 10 times its initial length, ⟨(iii) zero stress (×5 to ×6)⟩ indicates a film after relaxation, and ⟨(iv) drawing again (×10)⟩ indicates a film drawn to 10 times its initial length for a second time.

https://dx.doi.org/10.1021/acsomega.0c05662
ACS Omega 2021, 6, 7387−7393

Figure 4 shows the stress−strain curves of the cycling tests. The stress−strain curve from (i) to (ii) is typical behavior, as

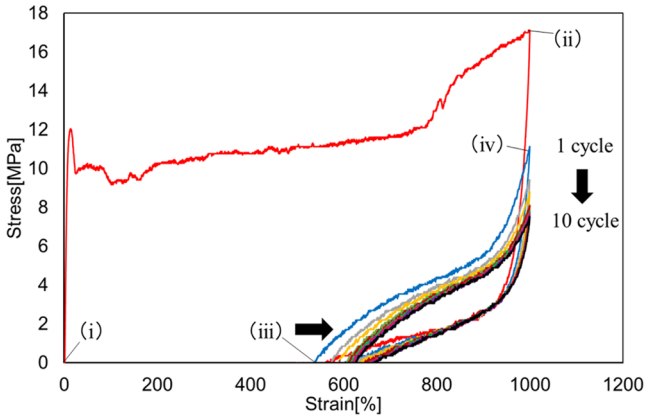

Figure 4. Stress−strain curves of the cycle test. The sample is the P(3HB-*co*-16 mol %-4HB) film undrawn. (i) Original (×1), (ii) drawing (×10), (iii) zero stress (×5 to ×6), and (iv) drawing again (×10) correspond to Figure 3. This graph shows 10 cycles highlighting the gradual shrinkage between cycles.

shown in Figure 2. In this region, necking-like drawing occurred. After the necking-like drawing, the strain increased markedly to 1000%. From (iii) to (iv), reversible cyclic behavior similar to that of rubber was found. However, this reversible elasticity was not perfect. The cycling area gradually shrank, indicating that the strain at zero stress gradually increased and the stress at 1000% strain gradually decreased. This shrinkage behavior stabilized after 20 cycles.

Figure 5 shows the change of the max stress and strain at zero stress at each cycle up to 60 cycles. The changes of both

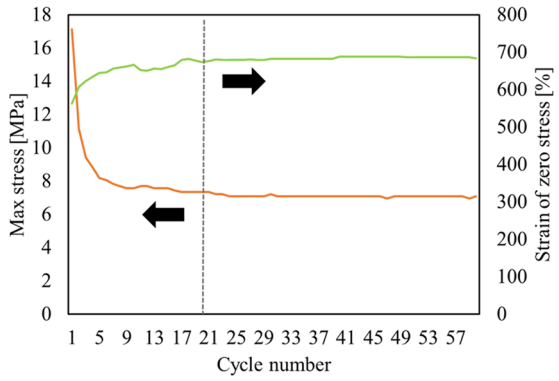

Figure 5. Max stress and strain at zero stress of each cycle. The graph shows 60 cycles. The orange line indicates the max stress, and the green line indicates the strain at zero stress. A dotted line near 20 cycles indicates the threshold of stable reversible elasticity.

the values of stress and strain became constant after 20 cycles, indicating that the film had stable reversible elasticity.

Synchrotron Wide-Angle X-ray Diffraction (WAXD) and Small-Angle X-ray Scattering (SAXS) Measurements. Figure 6 shows static-state WAXD and SAXS of the four different stage samples, as shown in Figure 3. Figure 7 shows *in situ* WAXD and SAXS images measured during stretching and shrinking. All of the WAXD and SAXD images measured at both static-state and *in situ* situations were almost the same. This result indicates that no relaxation had occurred

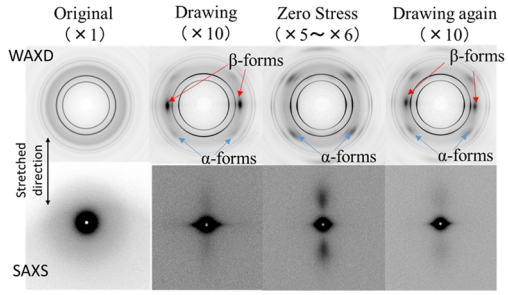

Figure 6. Wide-angle X-ray diffraction (upper panel) and small-angle X-ray scattering (lower panel) diagrams of P(3HB-*co*-16 mol %-4HB) films. (i) Original (×1), (ii) drawing (×10), (iii) zero stress (×5 to ×6), and (iv) drawing again (×10) correspond to Figure 3. Black arrows indicate the stretching direction of the films.

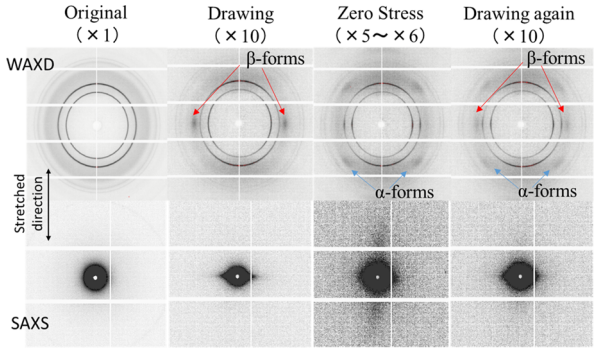

Figure 7. Time-resolved wide-angle X-ray diffraction (upper) and time-resolved small-angle X-ray scattering (lower) diagrams of P(3HB-*co*-16 mol %-4HB) films. (i) Original (×1), (ii) drawing (×10), (iii) zero stress (×5 to ×6), and (iv) drawing again (×10) correspond to Figure 3. Black arrows indicate the stretching direction of the films. Because of the continuous nature of the tests, the images appear as white slits.

during the experiments. Accordingly, these experimental results reflect the exact three-dimensional inner structural changes of the rubberlike elastic properties. In the case of the original sample, only ring patterns indexed by the α-form crystal (2/1 helix conformation crystal) were observed in WAXD, indicating that lamellar crystals exist randomly in solvent-cast films. After drawing to 10 times the original length, the α-form crystals were oriented along the stretching direction with the degree of orientation of 85%, and a new reflection was observed on the equatorial line assigned as the β-form crystal (the planar zigzag conformation crystal). However, there were no clear reflections in the SAXS images of either the original or films drawn to 10 times their initial length. This result indicates that β-form crystals were generated between lamellar crystals of α-form and that the lamellar crystal long-period of the oriented α-form crystals is not constant. The WAXD diagram of the zero-stress sample, which was released to the zero-stress state, shows that the reflection of the β-form on the equatorial line disappeared and that the intensity of the reflection of α-forms increased. Furthermore, two very clear reflections appeared along the meridian in the SAXS image. The orientation of α-form crystals was slightly increased to 88% by shrinkage of the tie molecular chains with a planar zigzag conformation (β-form). Taking the X-ray crystallinity into consideration, the long-period and the lamellar thickness of α-form crystals were calculated to be 10 and 2 nm, respectively. When the drawing was applied again to the zero-stress sample,

https://dx.doi.org/10.1021/acsomega.0c05662
ACS Omega 2021, 6, 7387−7393

the reflection of β-forms appeared again in WAXD and the two-spot reflections disappeared, as for the case of the first drawing of the films. This cycle of elongation (β-form, planar zigzag conformation) and shrinkage (random coil state) of tie molecular chains might cause rubberlike elasticity.

Figure 8a shows the changes of d-spacing calculated from the WAXD results at each stretching stage. The d-spacing was

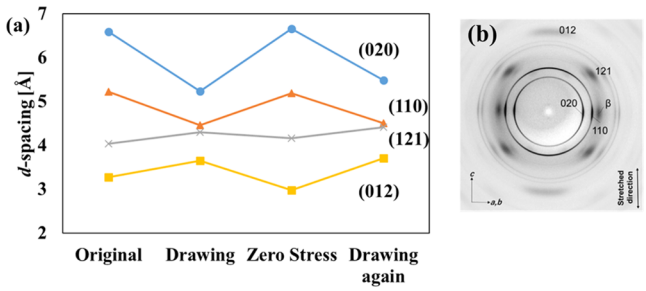

Figure 8. (a) Changes in the d-spacing of (020), (110), (121), and (012) reflections by time-resolved wide-angle X-ray diffraction diagrams of P(3HB-*co*-16 mol %-4HB) films. (i) Original (×1), (ii) drawing (×10), (iii) zero stress (×5 to ×6), and (iv) drawing again (×10) correspond to Figure 3. (b) X-ray fiber diagram of the drawing again sample, indicating mirror indices.

calculated by Bragg's law [$\lambda = 2d \sin\theta$] with mirror indices assigned in Figure 8b. In the cases of (020) and (110) on the equatorial line, the d-spacing decreased during drawing, indicating that the distance between the molecular chains along the b-axis was narrowed. In the cases of (121) and (012) on the layer lines, the d-spacing increased during drawing, indicating that the molecular chains were extended along the stretching direction by the rotation of the conformational angles.

On the basis of the changes in the d-spacings (Figure 8a), the changes of the crystal lattice size and fiber repeat distance were estimated. Figure 9 shows the changes of crystal lattice

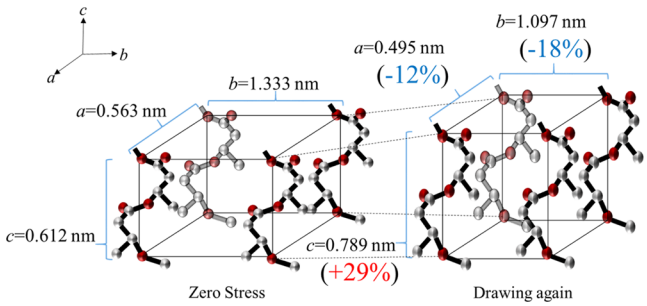

Figure 9. Deformation of the unit cell by changes in the d-spacing of (020), (110), (121), and (012) reflections in Figure 8. Zero stress and drawing again correspond to (iii) zero stress (×5 to ×6) and (iv) drawing again (×10) in Figure 3.

parameters calculated from the d-spacings determined from the (020), (110), and (012) reflections from the zero-stress to drawn-again states. The crystal lattice parameters at the zero-stress state were a = 0.563 nm, b = 1.333 nm, and c = 0.612 nm, which are very close to those of the normal P(3HB) lattice, a = 0.576 nm, b = 1.320 nm, and c = 0.596 nm.[20] However, the crystal lattice parameters at the drawn-again state markedly changed to a = 0.495 nm, b = 1.097 nm, and c = 0.789 nm. The rate of change of the a-axis and b-axis from the zero-stress state decreased by 12 and 18%, respectively. Conversely, the fiber repeat distance (c-axis) increased by 29%. These results indicate that the distance between the molecular chains along the a- and b-axes was reduced by stretching and that the fiber repeat distance was increased by rotation of the molecular conformation. Notably, the crystal volume slightly decreased from 0.459 to 0.428 nm^3 through the repeated drawing procedure. This result indicates that the crystal density was increased by decreasing the distance between molecular chains and the rotation of the conformational angles of the molecular chain.

When considering the stretching ratio of the film, the change from zero-stress to drawn-again states represented a change of 5 to 10 times the initial length. Thus, the entire film was stretched to be approximately twice its original length (*i.e.*, a 100% increase). The molecular chain length with a 2/1 helix conformation (α-form) accounts for 29% of the increase through rotation of the conformational angles. The remaining 71% increase is attributed to the generation of the β-form from the amorphous region between lamellar crystals of α-form crystals.

Mechanism of Reversible Elastic Properties of Crystalline Polymers. On the basis of these results, a new structural change model during elastic behavior is proposed in Figure 10. Nonoriented lamellar crystals of the α-form (2/1 helix conformation crystals) in solvent-cast films are aligned by the initial stretching. During stretching, β-form crystals with a planar zigzag conformation are generated between α-form crystals. However, because the lengths of the tie molecular chains are not identical, the long-period between α-form crystals was not the same. Accordingly, clear spotlike reflections were not observed in the SAXS images derived from the drawn films, as shown in Figures 6 and 7. However, when the stretching stress was released, interesting reflection patterns were observed in both the WAXD and SAXS images. The orientation of α-form crystals increased together with the appearance of strong two-spot reflections along the meridian in SAXS. Accordingly, β-forms might be returned to the amorphous phase by the release of stress, and α-forms remained highly oriented. When the drawing was repeated, tie molecular chains between the α-form crystals were again elongated. However, the periodicity of the lamellar crystals did not occur.

In summary, P(3HB-*co*-4HB) films can achieve a repeated zero-stress state and a drawn-again state. This is because the molecular chains in the amorphous region between lamellar crystals become β-forms through stretching and return to an amorphous phase on release. This behavior contributes to the reversible elasticity of P(3HB-*co*-4HB) films.

In addition, as shown in Figures 3 and 4, the cycle gradually shrank but stabilized after 20 cycles. This behavior can also be explained by these structural changes. The lamellar crystals (α-forms) orient by stretching, but this orientation process is not rapid. The lamellae gradually orient through cycle repetition. After 20 cycles, they are perfectly oriented and the film has stable reversible elasticity.

Tashiro et al.[26] and Perret et al.[27] proposed that parts of α-forms change to β-forms in P(3HB) melt-quench films and fibers, respectively. In the case of P(3HB-*co*-4HB), the 2/1 helix conformation (α-form) was slightly extended by 29% through rotation of the molecular conformation based on the calculated d-spacings in the WAXD fiber diagrams. The 4HB units in P(3HB-*co*-4HB) molecular chains mainly existed in

https://dx.doi.org/10.1021/acsomega.0c05662
ACS Omega 2021, 6, 7387−7393

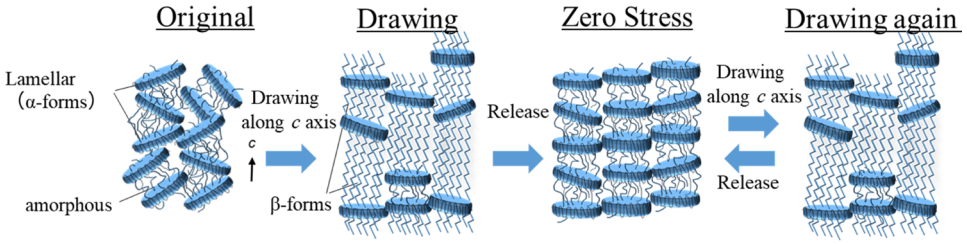

Figure 10. Conceptual diagram of the structural changes based on the results of WAXD and SAXS as shown in Figures 6 and 7. (i) Original (×1), (ii) drawing (×10), (iii) zero stress (×5 to ×6), and (iv) drawing again (×10) correspond to Figure 3. The conversion between zero stress and drawing again is repeatable.

amorphous regions. Accordingly, the stretching force was absorbed by changing the conformation angles of tie molecular chains in the amorphous region between lamellar crystals. As a result, the α-form in the crystal did not change to the β-form.

CONCLUSIONS

In this study, we used X-ray diffraction with synchrotron radiation to reveal the mechanism by which reversible elasticity of crystalline P(3HB-*co*-4HB) films is generated. Reversible elasticity is attributed to the combination of the generation of the β-form structure (planar zigzag conformation) from tie molecular chains in amorphous regions between lamellar crystals and extension of molecular chains in lamellar crystals (α-form) through rotation of the molecular conformation and orientation of lamellar crystals. Notably, P(3HB-*co*-4HB) has bioabsorbability and environmental biodegradability. Accordingly, this reversible elasticity is expected to be very useful for applications in biomaterials such as surgical sutures and scaffolds.

EXPERIMENTAL SECTION

Materials. Bacterial P(3HB-*co*-4HB) samples were supplied by Mitsubishi Gas Chemical. P(3HB-*co*-4HB) was biosynthesized from fructose and ε-caprolactone by *Cupriavidus necator*. All samples were used without further purification.

Characterization. The weight-average and number-average molecular weights (M_w and M_n) and polydispersity index (PDI) of the samples were measured using gel permeation chromatography (GPC) (RID-20A refractive index detector, Shimadzu) in chloroform at 40 °C. Shodex columns (K-806M, K-802) were used, and the flow rate was 0.8 mL/min. A calibration curve was constructed with the use of polystyrene (PS) standards (Shodex).

The 4HB content ratio was calculated by ^{1}H NMR. The ^{1}H NMR spectra were recorded using a JEOL JNM-A500 FT-NMR spectrometer (500 MHz) at room temperature. $CDCl_3$ was used as a solvent, and the chemical shifts are expressed relative to the resonance of tetramethyl silane.

The glass transition temperature and melting point were measured by differential scanning calorimetry (DSC). To confirm the melting behavior, differential scanning calorimetry (DSC) thermograms were recorded on a DSC8500 differential scanning calorimeter (Perkin Elmer) under a nitrogen atmosphere. The measurements were performed with 2−4 mg of the sample on a DSC pan. The sample was first heated from 30 to 200 °C at 20 °C/min in the first run, then cooled from 250 to −50 °C at 200 °C/min. Finally, scanning was performed with heating from −50 to 200 °C at a rate of 20 °C/min in a second run.

Film Preparation and Drawing. All samples were dissolved (0.025 g/mL) in chloroform at room temperature. The prepared solutions were transferred to 4.5 cm diameter Teflon Petri dishes and maintained at room temperature for 3 days to allow for gradual evaporation of the solvent. The solvent-cast films with a width of 3 mm and a thickness of 0.1 mm were drawn to 10 times their initial length by a stretching machine and released to a state of zero stress. The films were then drawn 10 times again at room temperature to confirm the drawing behavior of the films.

Stress−Strain Cycle Testing. Stress−strain curves were measured using a tensile testing machine (EZ-test, Shimadzu Co., Japan) at room temperature. The stretching rate was 20 mm/min, and the original length was 10 mm. The samples were cut into strips. The stress was calculated as the force divided by the initial area of the sample. The strain was calculated as the clump−clump distance during deformation divided by the original sample length. Mechanical properties were calculated from the values of at least five samples. The cycles of extension/retraction uniaxial deformation were applied with a maximum strain of 10 times their initial length and a minimum strain of five times their initial length.

Synchrotron Wide-Angle X-ray Diffraction and Small-Angle X-ray Scattering Measurements. Wide-angle X-ray diffraction (WAXD) and small-angle X-ray scattering (SAXS) measurements were performed at the BL45XU, BL40B2, and BL03XU beamlines in SPring-8 (Harima, Japan) with a wavelength of 0.1 nm. The sample-detector distances were 250 and 2500 mm for WAXD and SAXS, respectively. The X-ray diffraction patterns were recorded with a PILATUS. The diffraction angles were calibrated with the Debye−Scherrer ring of silicon and silver behenate for WAXD and SAXS measurements, respectively. In addition, *in situ* wide-angle and small-angle X-ray scattering measurements were performed under the same conditions. The films were mounted on a stretching machine and stretched at a controlled rate of 20 mm/min. The original length of the films was 10 mm.

AUTHOR INFORMATION

Corresponding Author

Tadahisa Iwata − *Science of Polymeric Materials, Department of Biomaterial Sciences, Graduate School of Agriculture and Life Science, The University of Tokyo, Tokyo 113-8657, Japan; Materials Visualization Photon Science Group, RIKEN, SPring-8 Center, Sayo-gun, Hyogo 679-5148, Japan;* orcid.org/0000-0003-2731-3958; Phone: +81-3-5841-5266; Email: atiwata@g.ecc.u-tokyo.ac.jp

https://dx.doi.org/10.1021/acsomega.0c05662
ACS Omega 2021, 6, 7387−7393

Authors

Yuki Kawamura − *Science of Polymeric Materials, Department of Biomaterial Sciences, Graduate School of Agriculture and Life Science, The University of Tokyo, Tokyo 113-8657, Japan; Materials Visualization Photon Science Group, RIKEN, SPring-8 Center, Sayo-gun, Hyogo 679-5148, Japan*

Hongyi Gan − *Science of Polymeric Materials, Department of Biomaterial Sciences, Graduate School of Agriculture and Life Science, The University of Tokyo, Tokyo 113-8657, Japan; Materials Visualization Photon Science Group, RIKEN, SPring-8 Center, Sayo-gun, Hyogo 679-5148, Japan*

Taizo Kabe − *Science of Polymeric Materials, Department of Biomaterial Sciences, Graduate School of Agriculture and Life Science, The University of Tokyo, Tokyo 113-8657, Japan; Materials Visualization Photon Science Group, RIKEN, SPring-8 Center, Sayo-gun, Hyogo 679-5148, Japan; Materials Structure Group I, The Research and Utilization Division, Japan Synchrotron Radiation Research Institute (JASRI), Sayo-gun, Hyogo 679-5148, Japan;* orcid.org/0000-0001-8417-2616

Akira Maehara − *Niigata Research Laboratory, Mitsubishi Gas Chemical co., Inc., Niigata 950-3112, Japan*

Satoshi Kimura − *Science of Polymeric Materials, Department of Biomaterial Sciences, Graduate School of Agriculture and Life Science, The University of Tokyo, Tokyo 113-8657, Japan; Materials Visualization Photon Science Group, RIKEN, SPring-8 Center, Sayo-gun, Hyogo 679-5148, Japan*

Takaaki Hikima − *Research Infrastructure Group, RIKEN, Harima Institute/SPring-8 Center, Sayo-gun, Hyogo 679-5148, Japan*

Masaki Takata − *Materials Visualization Photon Science Group, RIKEN, SPring-8 Center, Sayo-gun, Hyogo 679-5148, Japan; Institute of Multidisciplinary Research for Advanced Materials (IMRAM), Tohoku University, Sendai 980-8577, Japan*

Complete contact information is available at: https://pubs.acs.org/10.1021/acsomega.0c05662

Notes

The authors declare no competing financial interest.

■ ACKNOWLEDGMENTS

This work was partially supported by a Grant-in-Aid for Challenging Exploratory Research of JSPS (No. 180600000511 (T.I.)). The synchrotron radiation experiments were performed at the BL45XU of SPring-8 with the approval of RIKEN (Proposal No. 20180079), BL40B2 of SPring-8 (Proposal Nos. 2019A1213 and 2019B1018), and BL03XU of SPring-8 with the approval of FSBL (Proposal Nos. 2019A7234 and 2019B7270).

■ REFERENCES

(1) Alper, R.; Lundgren, D. G.; Marchessault, R. H.; Cote, W. A. Properties of poly-β-hydroxybutyrate. I. General considerations concerning the naturally occurring polymer. *Biopolymers* **1963**, *1*, 545−556.

(2) Anderson, A. J.; Dawes, E. A. Occurrence, Metabolism, Metabolic Role, and Industrial Uses of Bacterial Polyhydroxyalkanoates. *Microbiol. Rev.* **1990**, *54*, 450−472.

(3) Holmes, P. A. *Developments in Crystalline Polymers*; Elsevier Applied Science, 1988; pp 1−65.

(4) Saito, Y.; Nakamura, S.; Hiramitsu, M.; Doi, Y. Microbial Synthesis and Properties of Poly(3-Hydroxybutyrate-Co-4-Hydroxybutyrate). *Polym. Int.* **1996**, *39*, 169−174.

(5) Brandrup, J.; Immergut, E. H. *Polymer Handbook*, 2nd ed.; John Wiley and Sons, 1975.

(6) de Koning, G. J. M.; L, P. J. Crystallization phenomena in bacterial poly[(*R*)-3-hydroxybutyrate]: 2. Embrittlement and rejuvenation. *Polymer* **1993**, *34*, 4089−4094.

(7) Scandola, M.; Ceccorulli, G.; P, M. P. The physical aging of bacterial poly(D-β-hydroxybutyrate). *Macromol. Chem. Rapid Commun.* **1989**, *10*, 47−50.

(8) Kunioka, M.; Doi, Y. Thermal Degradation of Microbial Copolyesters: Poly(3-Hydroxybutyrate-*co*-3-Hydroxyvalerate) and Poly(3-Hydroxybutyrate-*co*-4-Hydroxybutyrate). *Macromolecules* **1990**, *23*, 1933−1936.

(9) Tanaka, T.; Fujita, M.; Takeuchi, A.; Suzuki, Y.; Uesugi, K.; Ito, K.; Fujisawa, T.; Doi, Y.; Iwata, T. Formation of Highly Ordered Structure in Poly[(*R*)-3-Hydroxybutyrate-*co*-(*R*)- 3-Hydroxyvalerate] High-Strength Fibers. *Macromolecules* **2006**, *39*, 2940−2946.

(10) Iwata, T.; Doi, Y. Mechanical Properties of Uniaxially Cold-Drawn Films of Poly[(*R*)-3-Hydroxybutyrate] and Its Copolymers. *Macromol. Symp.* **2005**, *224*, 11−19.

(11) Orts, W. J.; Marchessault, R. H.; Bluhm, T. L.; H, G. Observation of Strain-Induced Form in Poly (S-hydroxyalkanoates). *Macromolecules* **1990**, *23*, 5368−5370.

(12) Shimamura, E.; Kasuya, K.; Kobayashi, G.; Shiotani, T.; Shima, Y.; Doi, Y. Physical Properties and Biodegradability of Microbial Poly(3-Hydroxybutyrate-*co*-3-Hydroxyhexanoate). *Macromolecules* **1994**, *27*, 878−880.

(13) Doi, Y.; Kitamura, S.; Abe, H. Microbial Synthesis and Characterization of Poly(3-Hydroxybutyrate-*co*-3-Hydroxyhexanoate). *Macromolecules* **1995**, *28*, 4822−4828.

(14) Fischer, J. J.; Aoyagi, Y.; Enoki, M.; Doi, Y.; Iwata, T. Mechanical Properties and Enzymatic Degradation of Poly([*R*]-3-Hydroxybutyrate-*co*-[*R*]-3-Hydroxyhexanoate) Uniaxially Cold-Drawn Films. *Polym. Degrad. Stab.* **2004**, *83*, 453−460.

(15) Doi, Y.; Segawa, A.; Kunioka, M. Biosynthesis and Characterization of Poly(3-Hydroxybtyrate-*co*-4-Hydroxybtyrate) in Alcaligenes-Eutrophus. *Int. J. Biol. Macromol.* **1990**, *12*, 106−111.

(16) Saito, Y.; Doi, Y. Microbial Synthesis and Properties of Poly(3-Hydroxybutyrate-*co*- 4-Hydroxybutyrate) in Cornarnonas Acidovorans. *Int. J. Biol. Macromol.* **1994**, *16*, 99−104.

(17) Martin, D. P.; Williams, S. F. Medical Applications of Poly-4-Hydroxybutyrate: A Strong Flexible Absorbable Biomaterial. *Biochem. Eng. J.* **2003**, *16*, 97−105.

(18) Cong, C.; Zhang, S.; Xu, R.; Lu, W.; Yu, D. The Influence of 4HB Content on the Properties of Poly(3-Hydroxylbutyrate-*co*-4-Hydroxylbutyrate) Based on Melt Molded Sheets. *J. Appl. Polym. Sci.* **2008**, *109*, 1962−1967.

(19) Ying, T. H.; Ishii, D.; Mahara, A.; Murakami, S.; Yamaoka, T.; Sudesh, K.; Samian, R.; Fujita, M.; Maeda, M.; Iwata, T. Scaffolds from Electrospun Polyhydroxyalkanoate Copolymers: Fabrication, Characterization, Bioabsorption and Tissue Response. *Biomaterials* **2008**, *29*, 1307−1317.

(20) Yokouchi, M.; Chatani, Y.; Tadokoro, H.; Teranishi, K.; Tani, H. Structural Studies of Polyesters: 5. Molecular and Crystal Structures of Optically Active and Racemic Poly (β-Hydroxybutyrate). *Polymer* **1973**, *14*, 267−272.

(21) Okamura, K.; Marchessault, R. H. *Conformation of Biopolymers*; Academic Press: New York, 1967; Vol. *2*, pp 709−720.

(22) Iwata, T.; Aoyagi, Y.; Fujita, M.; Yamane, H.; Doi, Y.; Suzuki, Y.; Takeuchi, A.; Uesugi, K. Processing of a Strong Biodegradable Poly[(*R*)-3-Hydroxybutyrate] Fiber and a New Fiber Structure Revealed by Micro-Beam x-Ray Diffraction with Synchrotron Radiation. *Macromol. Rapid Commun.* **2004**, *25*, 1100−1104.

(23) Aoyagi, Y.; Doi, Y.; Iwata, T. Mechanical Properties and Highly Ordered Structure of Ultra-High-Molecular-Weight Poly[(*R*)-3-Hydroxybutyrate] Films: Effects of Annealing and Two-Step Drawing. *Polym. Degrad. Stab.* **2003**, *79*, 209−216.

(24) Iwata, T.; Tsunoda, K.; Aoyagi, Y.; Kusaka, S.; Yonezawa, N.; Doi, Y. Mechanical Properties of Uniaxially Cold-Drawn Films of Poly([*R*]-3-Hydroxybutyrate). *Polym. Degrad. Stab.* **2003**, *79*, 217−224.
(25) Iwata, T.; Fujita, M.; Aoyagi, Y.; Doi, Y.; Fujisawa, T. Time-Resolved X-Ray Diffraction Study on Poly[(*R*)-3-Hydroxybutyrate] Films during Two-Step-Drawing: Generation Mechanism of Planar Zigzag Structure. *Biomacromolecules* **2005**, *6*, 1803−1809.
(26) Phongtamrug, S.; Tashiro, K. X-Ray Crystal Structure Analysis of Poly(3-Hydroxybutyrate) β-Form and the Proposition of a Mechanism of the Stress-Induced α-to-β Phase Transition. *Macromolecules* **2019**, *52*, 2995−3009.
(27) Perret, E.; Reifler, F. A.; Gooneie, A.; Hufenus, R. Tensile Study of Melt-Spun Poly(3-Hydroxybutyrate) P3HB Fibers: Reversible Transformation of a Highly Oriented Phase. *Polymer* **2019**, *180*, No. 121668.

https://dx.doi.org/10.1021/acsomega.0c05662
ACS Omega 2021, 6, 7387−7393